Final Technical Report

USGS Award G10AP00018

"DYNAMIC MODELING OF M_W 7.0 EARTHQUAKES ON THE SIERRA MADRE – CUCAMONGA FAULT SYSTEM AND ITS IMPLICATIONS FOR STRONG GROUND MOTIONS IN GREATER LOS ANGELES: EFFECTS OF INELASTIC OFF-FAULT RESPONSE"

P.I. Shuo Ma
Department of Geological Sciences
San Diego State University
5500 Campanile Dr.
San Diego, CA 92182-1020

Phone: (619) 594-3091
Fax: (619) 594-4372
Email: sma@geology.sdsu.edu

Research supported by the U.S. Geological Survey (USGS), Department of the Interior, under USGS award number G10AP00018. The views and conclusions contained in this document are those of the authors and should not be interpreted as necessarily representing the official policies, either expressed or implied, of the U.S. Government.

Abstract

The Sierra Madre – Cucamonga fault system at the northern edge of the Los Angeles Basin, accommodates an important component of convergent motion across the southern Transverse Ranges and poses a significant seismic threat to metropolitan Los Angeles. In this project we modeled the same two M_w 7.7 scenario earthquakes (reported in 08HQGR0013) by incorporating the non-planar dipping fault geometry from the SCEC community fault model and 3D crustal velocity structure from the SCEC Community Velocity Model. The model setup is identical to the elastic simulations except that we included the inelastic off-fault response by using a Drucker-Prager yield criterion. The inelastic simulations assuming a relatively low cohesion value of 5 MPa show that the ground motions are slightly reduced by the inelastic response with the larger reduction near the fault. We found the nearly same ground motion patterns: the near-fault ground motion reaches up to 7 m/s on the hanging wall and ground motion in the Los Angeles basin can be as large as 3 m/s due to the basin-channeling effects. Both the up-dip and along-strike rupture directivity are not strong, similar to the previous elastic simulations. These results suggest that the fault geometry and 3D velocity structure play a more important role in determining ground motions than the inelastic off-fault deformation.

Publications resulting from this grant include:

Ma, S. and S. M. Day (2010), Dynamic modeling of Mw 7.0 or larger earthquakes on the Sierra Madre – Cucamonga fault system in Los Angeles: Effects of inelastic off-fault response, *Seism. Res. Lett.*, 81, 320.

Dynamic Modeling of M_w 7.0 Earthquakes on the Sierra Madre – Cucamonga Fault System and Its Implications for Strong Ground Motions in Greater Los Angeles: Effects of Inelastic Off-Fault Response

In a previously funded project (08HQGR0013) we quantified the seismic hazard posed by the Sierra Madre – Cucamonga fault system (Figure 1) by carrying out elastic simulations for two M_W 7.7 scenario earthquakes using a finite-element method. We incorporated the non-planar geometry of the fault system (Figure 2) from the SCEC Community Fault Model (Plesch et al., 2007) and the 3D heterogeneous velocity structure from the SCEC Community Velocity Model 4.0 (Magistrale et al., 2000). The simulations used about 1.2 billion finite elements and ground motion was simulated up to 0.5 Hz. We found large ground motions near the fault, where the ground motion on the hanging wall (San Gabriel Mountains) reaches about 7 m/s. Ground motion in some specific areas of the Los Angeles basin is as large as 3 m/s. The directivity effect was found not very strong. The peak ground velocity in the basin is in general less than 1 m/s. We refer the details of results to the report for 08HQGR0013.

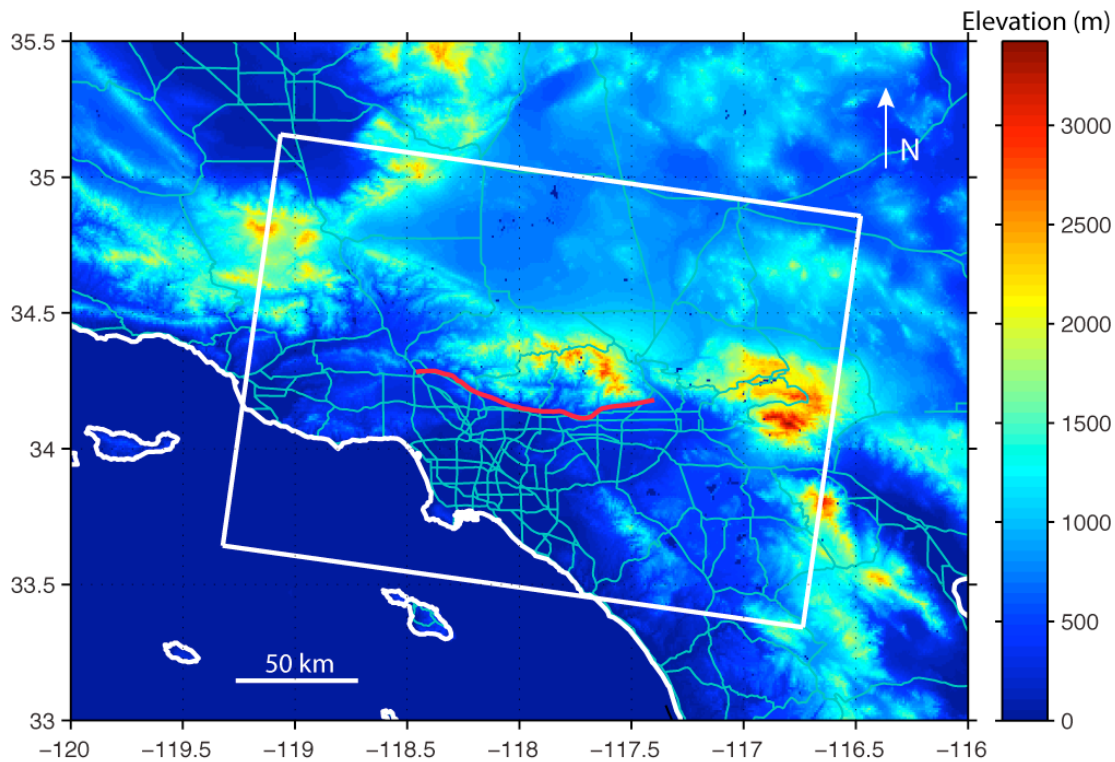

Figure 1. Topographic map of southern California. The trace of the Sierra Madre – Cucamonga Fault system is shown in red. White rectangle shows the area we include in the finite-element simulations. Major roads in the area are depicted in blue lines.

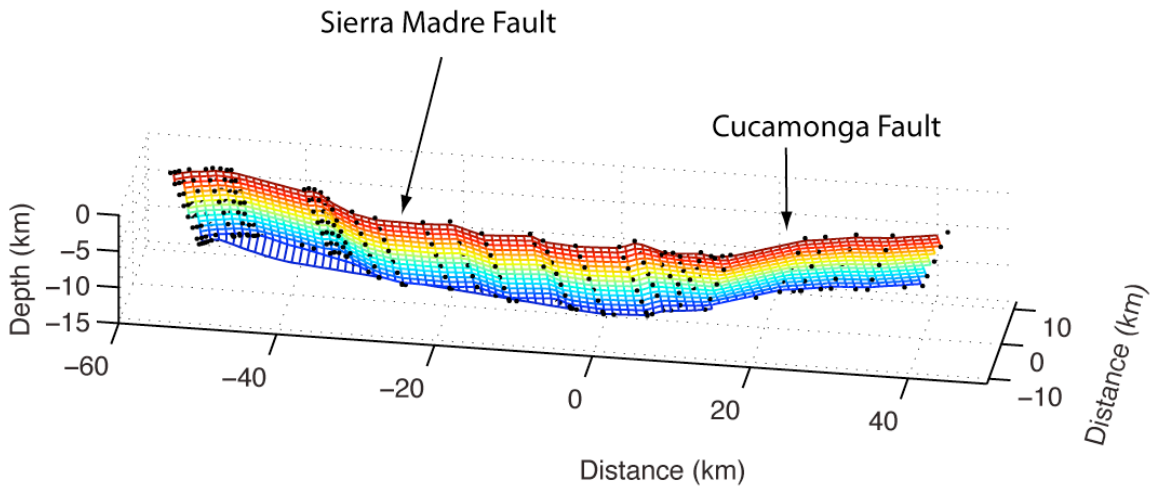

Figure 2. Geometry of the Sierra Madre – Cucamonga fault. The black dots are the defining points for the fault geometry in the SCEC Community Fault Model. A linear interpolation is used to generate the fault surface mesh.

In an elastic simulation of dynamic rupture on a fault, only tractions on fault (shear and normal tractions) are important in determining the rupture initiation, propagation, and healing, thus affecting seismic radiation. The off-fault stresses do not affect the elastic source process. It has been realized recently, however, that the off-fault stress changes (especially the fault-parallel stress component) in an elastic simulation are typically much larger, and can reach an order of magnitude higher, than the change of shear traction on fault (Poliakov et al., 2002; Rice et al., 2005; Andrews, 2005). Such large off-fault stress changes can create inelastic off-fault response.

The irrecoverable deformation off the fault due to earthquake ruptures is observed extensively in geologic records. A fault core, centimeters thick, with extremely fine-grained ultraclasite is often found in the fault zone of mature strike-slip faults. The core is bordered by a meters-wide zone of granulated material and, in turn, by hundreds of meters of fractured rock where the fracture density decreases to the background level (e.g., Chester et al., 1993).

We modeled the inelastic off-fault response in three dimensions for a strike-slip fault (Ma, 2008; Ma and Andrews, 2010). By using a pressure-dependent Drucker-Prager yield criterion (Drucker and Prager, 1952) in a depth-dependent stress environment, we demonstrated the significant effect of depth-dependent yielding. Because the confining pressure increases with depth, yielding occurs more easily near the surface than at depth. For low-cohesion materials (≤ 5 MPa), the inelastic strain confines narrowly to the fault at depth, but broadens dramatically near the surface, forming a 'flower-like' fault structure, which provides a physical interpretation to the formation of the low-velocity fault zone observed by fault-zone trapped waves (e.g., Li et al, 1990; Ben-Zion et al., 2003; Vidale and Li, 2003; Peng and Ben-Zion, 2006; Cochran et al., 2009).

In this project, we focused on the possible effects of inelastic off-fault response on ground motion estimates obtained by the elastic earthquake simulations on the Sierra Madre – Cucamonga fault system. The model parameters are identical to the elastic simulations, except that we allowed the off-fault response to be inelastic when it violates a yield criterion.

We incorporated the Drucker-Prager yield criterion (Drucker and Prager, 1952) in the finite-element simulations. This criterion is widely used in the rock and soil mechanics to describe the material failures. Similar to the Mohr-Coulomb yield criterion, yielding in this criterion also depends on the mean normal stress. The Drucker-Prager yield criterion is given as follows

$$\tau_v = \sqrt{0.5 s_{ij} s_{ij}}\,,$$

$$\tau_v^y = -\sigma_{kk}/3\sin\phi + c\cos\phi\text{, and}$$

$$\tau_v \le \tau_v^y, \tag{1}$$

where s_{ij} is the deviatoric stress, τ_v relates to the second invariant of deviatoric stress tensor ($0.5 s_{ij} s_{ij}$) and is regarded as a measure of the shear stress in the 3D stress state, c is the cohesion, φ is the internal frictional angle, τ_v^y is the yield stress, and the summation over repeated indices is assumed. In the principal stress space, the Drucker-Prager yield surface has the shape of a cone (Figure 3), representing the pressure-dependence of yielding. In this work, we assumed that the cohesion is 5 MPa and the internal friction is 0.75 everywhere for simplicity.

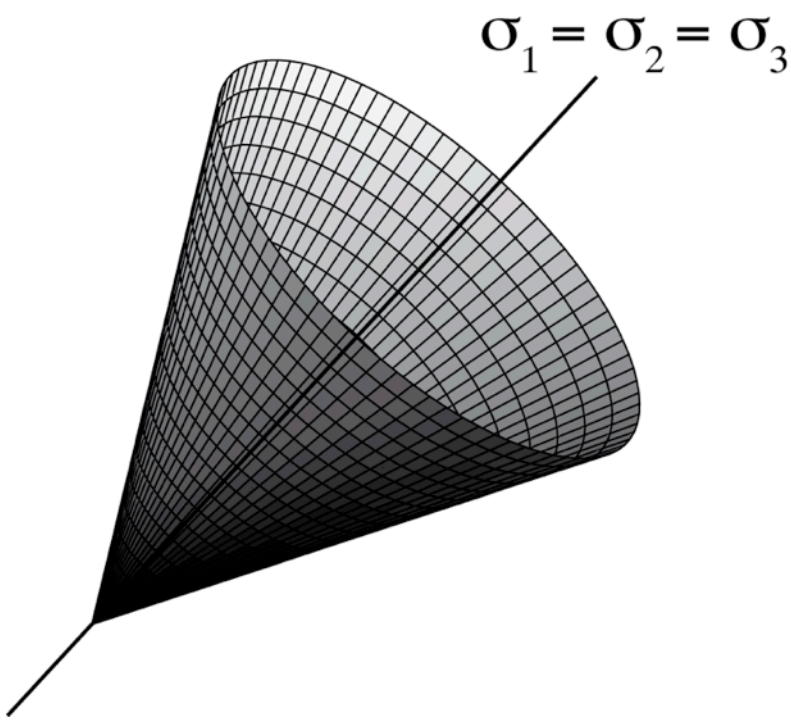

Figure 3. The yield surface of the Drucker-Prager yield criterion.

For inelastic simulations stresses need to be known everywhere in the volume to evaluate the yield criterion. We assumed a simple stress environment, which is the same as what we used in the elastic simulations. The maximum compressive stress, σ_1, is N8°E and has a depth gradient 38.87 MPa/km and the minimum compressive stress, σ_3, is vertical and the

depth gradient is 16.66 MPa/km. The intermediate principal stress, σ_2, is E8°S and has the relation $\sigma_2 = (\sigma_1 + \sigma_3)/2$. All the stresses are depth-dependent. The initial stresses on the fault are obtained by resolving the three principal stresses onto the nonplanar fault geometry, shown in Figure 4. Our assumption for the stress environment is consistent with existing stress measurements in southern California (Townend and Zoback, 2004), implying a weak San Andreas Fault (SAF) because the maximum compressive stress σ_1 is at a high angle to the San Andreas Fault.

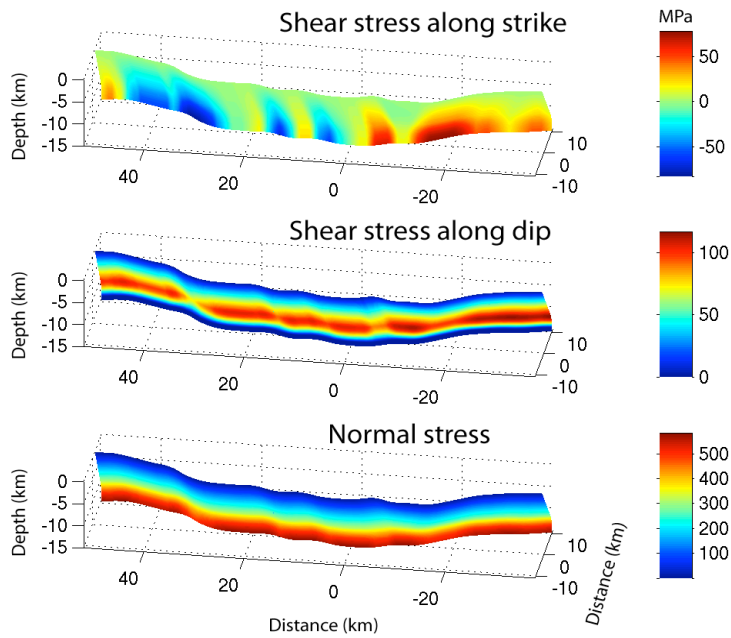

Figure 4. Initial stresses assumed in the simulations are mapped on the fault.

The peak ground velocity (PGV) maps for two rupture scenarios are illustrated in Figure 5, which are very similar to the PGV maps obtained in previous elastic simulations.

For the rupture scenario propagating from east to west (Figure 5a), large ground motions are concentrated at distances very close to the fault as well as in the Los Angeles basin. The large vertical motion is mostly located in a narrow band (~10 km wide) on the hanging wall, where the peak ground velocity (PGV) reaches about 7 m/s. The large horizontal ground motion is, however, on the footwall. The distribution of PGV in the basin is very similar to one of the Terashake scenarios (Olsen et al., 2008) where the rupture propagates from southeast to the northwest on the SAF, which leads to the similar excitation of basins. The seismic energy (dominated by the basin surface waves) channels through the San Bernardino Valley, Chino Basin and Los Angeles Basin, resulting in large amplification in certain areas where the ground motion reaches ~ 3 m/s. The velocity structure plays an important role in determining the ground motion levels. In the basin outside these specific areas, the ground velocity is in general less than 1 m/s, as clearly seen in the vertical component and one horizontal component (E8°S).

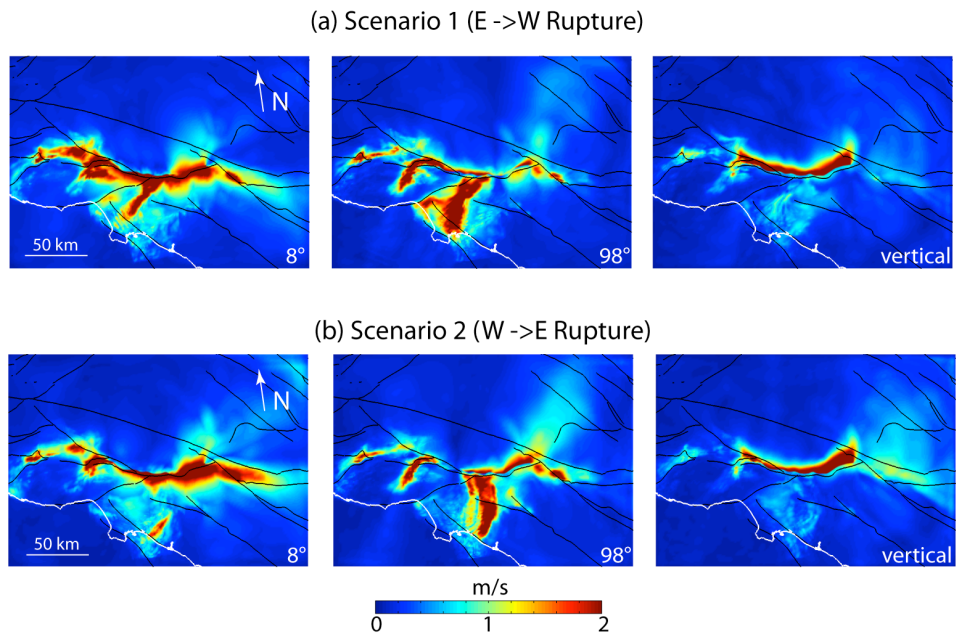

Figure 5. Distributions of PGV in the inelastic simulations are mapped on the surface for two different rupture scenarios. Major faults in the area are shown in black lines. Large ground motions are located near the fault as well as in the Los Angeles basin. The color scale is saturated in order to better illustrate features. The large vertical ground motion is mostly located in a narrow band on the hanging wall where it reaches 7 m/s. The ground motion in the basin reaches 3 m/s in some specific areas, while it is in general less than 1 m/s outside these areas. The rupture directivity effect is not very strong.

A similar pattern is observed for a scenario where rupture propagates predominantly from the west to the east (Figure 5b). A similar level of ground motion is seen in the San Fernando Valley and San Bernardino Basin. This demonstrates that for this scenario, effects of the velocity structure are more important than source directivity. The relatively weak directivity effect is attributable to the fact that the direction of rupture propagation (along strike) is not aligned with the slip direction (oblique slip) in large reverse earthquakes, as seen in the 1999 Chi-Chi earthquake (Aagaard et al., 2004). The amplification pattern in the Los Angeles basin is different as the excitation of the basin is different in these two rupture scenarios.

The up-dip directivity is also not very strong. The PGV in most areas in the basin is less than 1 m/s. The small up-dip directivity is due to the limited up-dip propagation distance. This is also consistent with the observation in the 2008 Wenchuan earthquake that the populated Sichuan basin did not suffer much damage even though it is located in the up-dip direction of the Longmen Shan Fault system.

Figure 6 compares the cross sections of the PGV along N8°E between the elastic and inelastic simulations. The PGV values are only reduced slightly by the inelastic off-fault response, which explains the similarity of the PGV maps between the elastic and inelastic simulations. The largest reduction (~30%) is observed near the fault. These results suggest that the inelastic off-fault response plays an insignificant role in affecting ground motions in the Los Angeles basin compared to the fault geometry and the 3D velocity structure. The cohesion value we chose is small (5 MPa) corresponding to sedimentary rocks. If the cohesion value is larger the effect of the inelastic off-fault response will be even smaller.

The effect of inelastic off-fault response on ground motions, however, needs more work. Significant effects have been shown in 2D simulations using fine resolution grids (e.g., Andrews et al., 2007; Ma, 2009). One possible reason that we did not see a large effect of inelastic off-fault response on ground motions might be due to the coarse resolution of the 3D simulations.

(a)

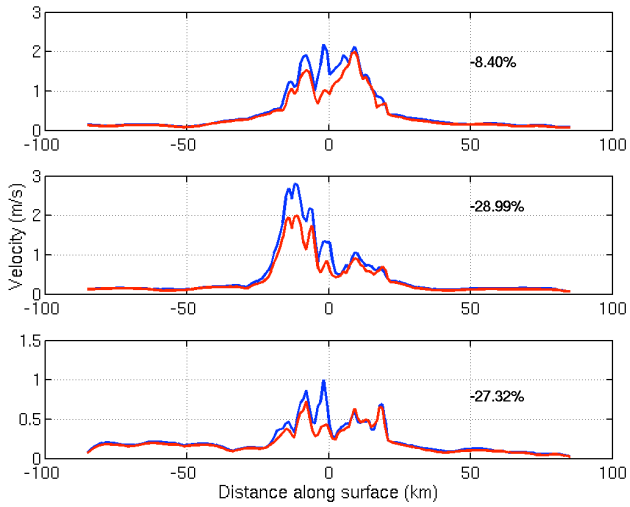

(b)

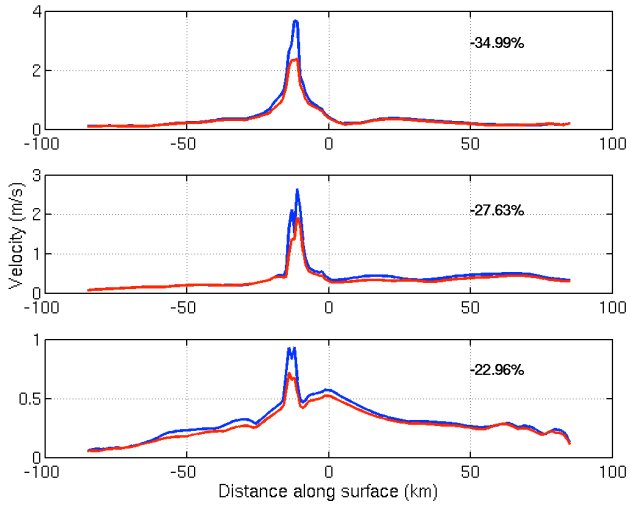

Figure 6. Comparisons of the PGV values at two cross sections (approximately perpendicular to the fault) between elastic (blue) and inelastic (red) simulations. The traces from top to bottom are fault-parallel (8°), fault-normal (98°), and vertical component, respectively. The percentage in each panel shows the relative reduction due to the inelastic off-fault response.

References:

Aagaard, B. T., J. F. Hall, and T. H. Heaton, Effects of fault dip and slip rake angles on near-source ground motions: why rupture directivity was minimal in the 1999 Chi-Chi, Taiwan, earthquake, *Bull. Seismol. Soc. Am.,* 94, 155-170, 2004.

Andrews, D. J. (2005), Rupture dynamics with energy loss outside the slip zone, J. Geophys. Res., 110, B01307, doi:10.1029/2004JB003191.

Andrews, D. J., T. C. Hanks, and J. W. Whitney (2007), Physical limits on ground motion at Yucca Mountain, Bull. Seismol. Soc. Am., 97, 1771-1792.

Ben-Zion, Y., Z. Peng, D. Okaya, L. Seeber, L. G. Armbruster, N. Ozer, A. J. Michael, S. Baris and M. Aktar (2003), A shallow fault zone structure illuminated by trapped waves in the Karadere-Duzce branch of the North Anatolian fault, western Turkey, *Geophys. J. Int.,* 152, 699–717, doi:10.1046/j.1365-246X.2003.01870.x.

Chester, F. M., J. P. Evans, and R. L. Biegel (1993), Internal structure and weakening mechanisms of the San Andreas fault, *J. Geophys. Res.*, 98, 771–786.

Cochran, E. S., Y-G Li, P. M. Shearer, S. Barbot, Y. Fialko, and J. E. Vidale (2009), Seismic and Geodetic evidence for extensive, long-lived fault damage zones, *Geology*, 37, 315-318, doi: 10.1130/G25306A.1.

Drucker, D. C. and W. Prager (1952), Soil mechanics and plastic analysis or limit design, Quart. Appl. Maths., **10,** 157 – 165.

Li, Y. G., P. C. Leary, K. Aki and P. E. Malin (1990), Seismic trapped modes in the Oroville and San Andreas fault zones, Science, 249, 763–766.

Ma, S. (2008), A physical model for widespread near-surface and fault zone damage induced by earthquakes, Geochem. Geophys. Geosyst., 9, Q11009, doi:10.1029/2008GC002231.

Ma, S. (2009), Distinct asymmetry in rupture-induced inelastic strain across dipping faulting: An off-fault yielding model, *Geophys. Res. Lett.*, 36, L20317, doi:10.1029/2009GL040666.

Ma, S., and D. J. Andrews (2010), Inelastic off-fault response and three-dimensional earthquake rupture dynamics on a strike-slip fault, *J. Geophys. Res.*, 115, B04304, doi:10.1029/2009JB006382.

Magistrale, H., S. M. Day, R. W. Calyton, and R. Graves (2000), The SCEC southern California reference three-dimensional seismic velocity model version 2, Bull. Seismol. Soc. Am. 90, S65-S76.

Olsen, K. B., S. M. Day, J. B. Minster, Y. Cui, A. Chourasia, D. Okaya, P. Maechling, and T. Jordan (2008), TeraShake2: Spontaneous rupture simulations of M_W 7.7 earthquakes on the southern San Andreas Fault, Bull. Seismol. Soc. Am., 98, 1162-1185.

Poliakov, A. N. B., R. Dmowska, and J. R. Rice (2002), Dynamic shear rupture interactions with fault bends and off-axis secondary faulting, J. Geophys. Res., 107(B11), 2295, doi:10.1029/2001JB000572.

Peng, Z. and Y. Ben-Zion (2006), Temporal Changes of Shallow Seismic Velocity around the Karadere-Duzce Branch of the North Anatolian Fault and Strong Ground Motion, PAGEOPH., 163, 567–599.

Plesch, A. and others (2007), Community Fault Model (CFM) for southern California, 97,

1793-1802.
Rice, J. R., C. G. Sammis, and R. Parsons (2005), Off-fault secondary failure induced by a dynamic slip pulse, Bull. Seismol. Soc. Am., 95, 109-134, doi: 10.1785/0120030166.
Townend, J., and M. D. Zoback (2004), Regional tectonic stress near the San Andreas fault in central and southern California, Geophys. Res. Lett., 31, L15S11, doi:10.1029/2003GL018918.

Vidale, J. E. and Y.-G. Li (2003), Damage to the shallow Landers fault from the nearby Hector Mine earthquake, *Nature*, 421, 524–526.